Journal of Controlled Release 286 (2018) 358–368

Contents lists available at ScienceDirect

Journal of Controlled Release

journal homepage: www.elsevier.com/locate/jconrel

Enhanced drug delivery using sonoactivatable liposomes with membrane-embedded porphyrins

Xiaobing Wang[a,b,1], Fei Yan[a,1], Xiufang Liu[a,1], Pan Wang[b], Shuai Shao[c], Yue Sun[b], Zonghai Sheng[a], Quanhong Liu[b], Jonathan F. Lovell[c], Hairong Zheng[a,*]

[a] Paul C. Lauterbur Research Center for Biomedical Imaging, Institute of Biomedical and Health Engineering, Shenzhen Institutes of Advanced Technology, Chinese Academy of Sciences, Shenzhen 518055, China
[b] Key Laboratory of Medicinal Resources and Natural Pharmaceutical Chemistry, Ministry of Education, College of Life Sciences, Shaanxi Normal University, Xi'an 710119, China
[c] Department of Biomedical Engineering, University at Buffalo, State University of New York, Buffalo, NY 14260, USA

ARTICLE INFO

Keywords:
Porphyrin-phospholipid-liposome
Ultrasound-responsive
Controlled release and deep penetration
Sonodynamic therapy

ABSTRACT

Small molecules that interfere with nucleic acid are widely used in chemotherapy, however, improved delivery approaches are required to improve anti-tumor outcomes. Here, we present the development of an ultrasound-activatable porphyrin-phospholipid-liposome (pp-lipo) that responds to low intensity focused ultrasound (LIFU) for sonodynamic therapy (SDT). The pp-lipo is constructed by incorporating a small proportion of porphyrin (pyropheophorbide) conjugated lipid into a liposome formulation. This enables sonosensitization-induced lipid oxidation and efficient disruption of liposomes to release loaded doxorubicin (Dox). This results in increased Dox nuclear subcellular location and cytotoxicity in cancer cells *in vitro* upon pp-lipo exposure to LIFU. Following intravenous administration, LIFU enhanced deposition of Dox within tumor tissue, suppressed tumor growth, and also increased porphyrin near infrared tumor fluorescence. Thus, pp-lipo is a versatile carrier that can be extended to many ultrasound-controllable drug delivery applications.

1. Introduction

Small molecules that bind DNA such as doxorubicin (Dox) have been intensively used in clinical cancer treatment, due to their anti-proliferative and pro-apoptotic effects [1]. However, non-specific distribution to other organs often results in dose-limiting toxicities that reduce their therapeutic potential [2]. Encapsulation of Dox and other DNA-damaging agents into a nanosized delivery system (NDS) alters the pharmacokinetics and distribution of these agents and thus, reduces their systemic cytotoxicity [3].

Several NDSs have been designed to specifically transport DNA-damaging agents to cancer cells, such as liposomes, polymeric micelles, and organic/inorganic nanoparticles. Among them, liposomes have attracted significant attention due to their unique physiochemical properties. Consequently, liposomes have been clinically approved to improve the biodistribution and anti-cancer efficiency of various drugs. Currently, about a dozen liposome-based drugs have been approved for clinical usage and several more are at different stages of clinical trials [4]. Doxil is a PEGylated liposome that has been approved for intravenous application with the composition of HSPC/cholesterol/DSPE-PEG2000 [5]. Although this liposome formulation has increased the blood circulation time, reduced several side effects of Dox, sufficient and uniform drug delivery is often hampered by physiological barriers and non-optimal drug bioavailability. To address this issue, several strategies have been explored with the aid of external stimuli that stimulate local drug deposit. These are based on heat, light, magnetism and ultrasound (US), all of which are feasible external practical applications for both research and clinical [6, 7]. Such stimuli-responsive platforms facilitate drug release at targeted sites in response to a specific stimulus, improving therapeutic efficiency [8, 9]. Among these external stimuli-responsive NDSs, light responsive systems have been investigated because they are not only non-invasive, but also can be controlled with high spatial and temporal precision [10]. Porphyrin is a well-known photoacoustic contrast material that has been explored as diagnostic and therapeutic agent for clinic trials [11, 12]. One approach is liposome-like porphysome [13]. Porphysome self-assembles from porphyrin-phospholipid with powerful drug loading ability and effectively mediated photothermal therapy, photodynamic therapy and

* Corresponding author.
E-mail address: hr.zheng@siat.ac.cn (H. Zheng).
[1] X. Wang, F. Yan, and X. Liu contributed equally to this work.

https://doi.org/10.1016/j.jconrel.2018.07.048
Received 17 May 2018; Received in revised form 6 July 2018; Accepted 31 July 2018
Available online 01 August 2018

multimodal imaging [14, 15]. Such porphyrin-based liposomes also displayed unique nanoscale optical properties, robust biocompatibility and high biodegradability, showing promising value for diverse biomedical applications [16, 17].

The limited penetration depth of light into biological tissues remains challenging [18]. On the one hand, US as a trigger of drug release has a unique advantage since it can propagate through deep tissue and its energy can be specifically focused into the target with minimal effects on surrounding normal tissues [19, 20]. In addition, the noninvasive and nonionizing features of US treatment enable repetitive stimuli without causing long-term cumulative effects [21]. Therefore, drug delivery *via* US is a promising trigger. Prior research towards the sound modulation of micelles and liposomes with sufficient intensities has been explored [22]. Schroeder et al. reported that drug release was attributed to the permanent destabilization of ~20% of all liposomes and the formation of transient pores in the remainder [23]. Ahmed et al. suggested low frequency US to be more efficient than high frequency US in inducing drug release from stealthy liposomes [24]. The lipid compositions have also been reported to influence the sonosensitivity with respect to drug release [25].

US would be a powerful physical modality for the spatiotemporal control of on-demand drug release. US-assisted drug delivery has made steady progress towards the clinic implementation. Although primary studies using low frequency unfocused US have indicated that sufficient cavitation is needed to release liposomal contents, developing US-responsive liposomes, especially response to therapeutic US, is also necessary to improve the sensitivity of liposomes to US. Porphyrins have been used as sonosensitizers to increase the efficiency of US and the combined sonodynamic therapy field is rapidly emerging [26, 27]. Porphyrin-based liposomes might respond to US triggering. Porphyrin-phospholipids offer the advantage of biologically stable incorporation into the liposome bilayer. In this study, we present the development of a sonosensitive porphyrin-phospholipid-liposome (pp-lipo) with stable drug loading. This pp-lipo releases the payload upon US exposure, thus assisting specific drug delivery to target tissues and cells. As a sonosensitizer, porphyrin is expected to reduce the US intensity required for drug release from the liposome. We show pp-lipo that be regulatable by low intensity focused ultrasound (LIFU) at a therapeutic frequency of 1.0 MHz, can precisely control DNA damage *in situ*. Pp-lipo was constructed by incorporating of two molar of pyropheophorbide-phospholipid (Pyro-lipid), which enabled tumor cellular uptake and resulted in rapid liposomal structure disruption. This stimulated ROS generation and enhanced sonochemotherapy upon US exposure (Fig.1).

2. Experimental section

2.1. Materials

Pyro-lipid was synthesized as previously described [13]. 1,2-distearoyl-sn-glycero-3-phosphocholine (DSPC), 1,2-distearoyl-sn-glycero-3-phosphoethanolamine-N-[methoxy (polyethylene glycol)-2000] (DSPE-PEG2000), dioleoylphosphatidylcholine (DOPC), and Cholesterol were obtained from Avanti Polar Lipids (Alabaster, USA). Doxrubicin, 4′,6-diamidino-2- phenylindole (DAPI), ethidium bromide (EB), 3-(4,5-dimethylthiazol-2-yl)-2,5-diphenyltetrazolium bromide (MTT), 2′,7′-dichlorodihydrofluorescein-diacetate (DCFH-DA), and sodium azide (NaN3) were purchased from Sigma-Aldrich (St. Louis, USA). Calcein-AM/PI Double Staining Kit was obtained from Yeasen (China). Cell Counting Kit-8 kit (CCK-8) was purchased from Dojindo Laboratories (Kumamoto, Japan).

2.2. Pp-lipo synthesis

Pp-lipo were prepared *via* thin film hydration method as previously reported [17]. The film consists of 51.5 mol% DSPC, 2 mol% Pyro-lipid, 40 mol% cholesterol, 5 mol% DSPE-PEG2000, and 1.5 mol% DOPC. Control liposomes without Pyro-lipid were prepared at the same time, containing DSPC/cholesterol/DSPE-PEG/DOPC at a molar ratio 53.5:40:5:1.5. The dried film was hydrated with PBS (pH 7.2) at a concentration of 10 mg/ml lipid and was then subjected to five times freeze-thaw cycles, by freezing the test tube in liquid nitrogen and thawing it in water heated to 65 °C. The liposomes were then downsized by stepwise extrusion (using a Mini-Extruder, Avanti Polar Lipids) through polycarbonate filters with pore sizes of 100 nm (Nuclepore, Whatman). Dox loading was achieved by adding a 1:5 weight ratio of drug: lipid and incubation at 60 °C for 1 h, driven by a transmembrane ammonium sulphate gradient (250 mM, pH 5.5) [28]. Free Dox was removed *via* dialysis. The entrapment efficiency of Dox was determined by fluorescence using a multimode microplate reader (Tecan, Switzerland). A Malvern Zeta sizer Nano ZS90 (Malvern Instrument, UK) was used to examine the mean size, polydispersity index, and zeta potential of different liposome groups. The morphology of nanoparticles was monitored by transmission electron microscopy (TEM). The porphyrin spectra were determined using a Perkin-Elmer spectrophotometer (USA). Stability studies showed little liposome leakage after four weeks of storage at 4 °C.

For release experiments, liposomes were exposed to US treatment at indicated intensities of 0.15 W/cm^2, 0.2 W/cm^2 and 0.3 W/cm^2 for variable durations. Cargo release was assessed by measuring the fluorescence intensity both before (F_0) and after treatment (F_1), including solubilization with 1% DMSO (F_D). The release was calculated using the following formula: release ratio = $(F_1 - F_0)/(F_D - F_0) \times 100\%$.

2.3. US exposure

The US exposure system used in this experiment consisted of an arbitrary-waveform signal generator (model AFG3102, Tektronix, USA), a power amplifier (AR150A100B, USA), and a focused transducer (ndtXducer®, Northborough, USA). The transducer was a piezoelectric composite and had matching layers and a thick backing. The transducer was 1.0 MHz with a focal length of about 5 cm. The acoustic field was characterized using a capsule hydrophone (onda HGL-0200, Onda, Sunnyvale, USA) that was connected to a 20-dB preamplifier (Onda AH-2020) in a rectangular Plexiglas water tank. A 5% duty cycle at 1 Hz repetition frequency in tone-burst mode was performed.

For sonication *in vitro*, cells or liposome suspensions were placed in the focal zone of the US transducer. The samples were exposed to US for 60 s duration with intensities of 0.15, 0.2, and 0.3 W/cm^2 (I_{SPTA}), respectively. To investigate the drug release as a function of exposure time, liposomes were exposed to US for a range of sonication times of 0–180 s at 0.2 W/cm^2. The temperatures of the samples were measured before and immediately after each US exposure using a digital thermometer. For *in vivo* experiments, the tumor region was rightly placed in the focus center of the transducer with assistance of a multilayer interface-material that improved the acoustic efficiency of delivery into the tumor.

2.4. Validation of acoustic cavitation

To investigate whether the utilized US parameters generated inertial cavitation, a terephthalate (TA) dosimeter was used. Briefly, when inertial cavitation occurs, the produced hydroxide radicals (OH) react with non-fluorescent terephthalate to form fluorescent 2-hydroxyterephthalic acid (HTA). TA solution (1×10^{-4} M) was placed in the sample chamber and exposed to various acoustic intensities as described above. The fluorescence intensity of each treatment was measured to obtain values with the same settings (Ex = 320 nm and Em = 430 nm). The background fluorescence intensity of TA was subtracted from the fluorescent intensity of HTA.

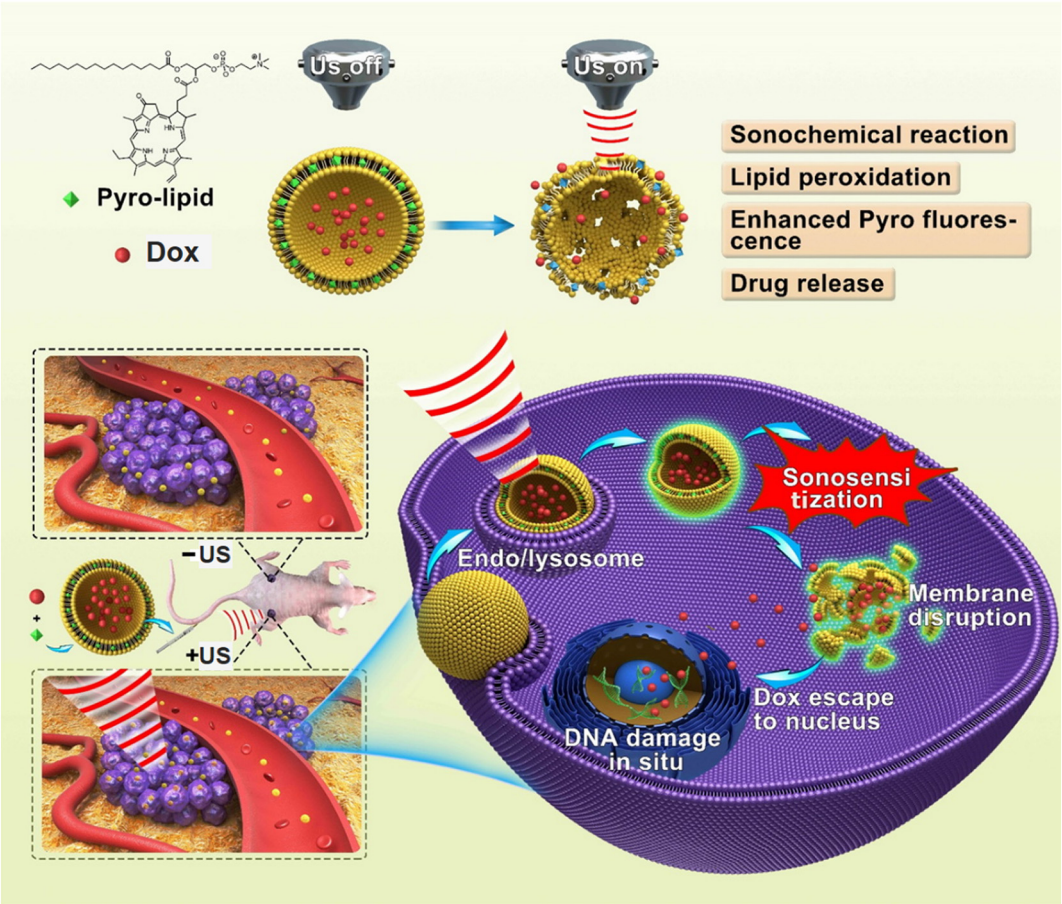

Fig. 1. Representation of sonoactivatable, Dox-loaded porphyrin-phospholipid-liposome (Dox-pp-lipo) for anti-tumor treatment.

2.5. TEM observation of liposomes

After different US treatments, samples were prepared by depositing a drop of the solutions (10 μl) onto carbon-coated copper grids and drying them at room temperature. Then, a small drop of phosphotungstic acid solution (2% wt in water, pH 7.4) was added to the copper grid. The grid was dried overnight (in a desiccator) prior to TEM observation using the Hitachi model JEM-1200 (Tokyo, Japan) operated at an accelerating voltage of 120 kV.

2.6. FT-IR (Fourier transform infrared) and mass spectrum detection

The FT-IR spectra of pp-lipo before and after US treatment were recorded using a FT-IR spectrometer (Nicolet iS10) in the range of 4000–400 cm^{-1}. The spectral resolution was 4 cm^{-1}. The Mass-spectrum was recorded using the AB Sciex 4000 QTRAP system spectrometer (SCIEX).

2.7. Cell culture and cellular uptake

U87 cells were cultured in Dulbecco's modified Eagle's medium with 10% fetal bovine serum and 1% antibiotic solution (GIBCO, Invitrogen). The cell suspension was transferred into an eight-well confocal chamber slider. After culture for 12–24 h, cells were visually examined by optical microscopy. 10 μg/ml Dox was then added to the cells in either free or liposomal form in opti-MEM (Gibco) for 2 h. The prepared pp-lipo with Dox encapsulation was named Dox-pp-lipo, and conventional liposomes without Pyro-lipid (named Dox-lipo) were used for comparison. The bottom of each well was then exposed to US for 60 s at an intensity of 0.2 W/cm^2. Then, cells were washed with cold PBS and fixed with 4% paraformaldehyde for 10 min and stained with DAPI for 5 min. Imaging was performed using a Leica TCS SP5 confocal microscopy.

2.8. In vitro cytotoxicity

In vitro cell studies were performed by seeding U87 cells in a 96-well plate. Different doses of Dox in free or liposomal forms were added to the Opti-MEM for 2 h. Then, wells were irradiated with the indicated US treatment. The media were left to incubate for 24 h and the CCK-8 assay was performed to assess the cytotoxicity of Dox-pp-lipo, using Dox-lipo as controls. The student's *t*-test was used to test the statistical significance. The synergistic effect of Dox-pp-lipo and US exposure on U87 cells was further verified using Calcein AM and PI staining according to the manufacturers' protocol. Cells were examined *via* biological inverted fluorescence microscope (Olympus IX71, JPN).

2.9. Assessment of DNA damage in vitro

US assisted DNA damage *in vitro* was assessed by single cell gel electrophoresis [29]. Briefly, after different US treatments (0.15 W/cm^2, 0.2 W/cm^2 and 0.3 W/cm^2), cells were mixed with 0.75% (w/v) low melting point agarose, bathed in lysing buffer for 0.5 h, and subjected to unwinding in alkaline solution. Electrophoresis was performed at 25 V for 20–30 min. After staining with EB, samples were observe with fluorescence microscope and analyzed with Comet Assay Software.

2.10. Intracellular ROS generation

Intracellular ROS production was determined by flow cytometry using DCFH-DA as previously reported [30]. All obtained data were

expressed as the percentage of cells with high fluorescence intensity of DCF among 10,000 cells.

2.11. In vivo fluorescence imaging

Animal experiments were conducted with approval of the Shenzhen Institutes of Advanced Technology, Chinese Academy of Sciences Animal Care and Use Committee. Tumor bearing BALB/c nude mice were established by subcutaneous injection of 5×10^6 U87 cells onto the hind flank of mice. After 1–2 weeks of growth, when tumors reached 5–6 mm in diameter, animals received pp-lipo injection through the tail vein (50 nmol Pyro-lipid). Then images were captured *via* an *in vivo* fluorescence at indicated time points with the mice under isoflurane-induced anesthesia.

To study the influence of US exposure on pp-lipo *in vivo*, tumors were irradiated for 3 min after 12 h of administration of pp-lipo, using 0.15, 0.2 and 0.3 W/cm^2 US, respectively. Whole body imaging was performed again under NIR region using the IVIS Spectrum Imaging System.

2.12. Ex-vivo fluorescence imaging

To analyze the biodistribution of Dox in response to US exposure, tumor-bearing mice were injected with 10 mg/kg Dox in either free or liposomal forms *via* the tail-veil. After 12 h, tumors were exposed to different US intensities. Then, mice were killed, tumors and organs of interest were harvested and visualized *via ex vivo* fluorescence system. To further compare the Dox accumulation in tumors after different US exposures, tumors were frozen in OCT gel and then sectioned and imaged by Stereo Fluorescence Microscope to preview their distribution pattern. Then, the frozen slides were stained with nuclei-dye DAPI and observed using fluorescence microscopy to distinguish Dox subcellular distribution *in situ*.

2.13. In vivo antitumor studies

The anti-tumor efficacy was evaluated using BALB/c nude mice (4 weeks old, 18–20 g) that were subcutaneously xenografted with U87 cells into the right thigh. After 1–2 week of tumor growth, the tumor volumes were approximately 60–80 mm^3, and tumor-bearing mice were ready for studies. Anti-tumor efficiency was evaluated by calculating the tumor size. Focused US was used to trigger pp-lipo at 12 h after different administrations. The lengths and widths of tumors were measured using vernier calipers and the tumor volume was calculated using the following equation: tumor volume (mm^3) = 0.5 × length × width × width. For survival studies, each group used five mice. The tumor-bearing mice were monitored every day, and the survival curve was calculated. Histopathological evaluation was also performed and tumor sections were stained with hematoxylin and eosin (HE) to evaluate tumor damage *in situ*. PCNA (Boster, China) and TUNEL (Roche, Switzerland) assays were used to analyze both the cellular proliferation inhibition and cell apoptosis, respectively, according to manufacturers' standard protocols.

3. Results and discussion

3.1. Formulation of pp-lipo and behavior of pp-lipo upon US exposure

Previous studies developed a robust stealthy porphyrin-phospholipid-liposome that showed long-circulation and that could be stimulated by NIR light to release encapsulated drugs [17]. Compared to NIR irradiation, US achieves much deeper penetration and its energy can be regulated in exposed areas [31]. Here, we aimed to explore the potential US-responsiveness of porphyrin-phospholipid-liposome and to elucidate the release mechanism. Transmission electron microscopy demonstrated a nearly spherical structure of Dox-pp-lipo and Dox-lipo (Fig. 2A). Light scattering measurements showed a mean diameter of ~100 nm with or without Pyro-lipid incorporation. The amount of Dox that was encapsulated in pp-lipo was determined spectrophotometrically as a 92% loading efficiency. The absorption and fluorescence spectra of Dox-pp-lipo is shown in Supporting Fig.1. Dox-pp-lipo showed two main porphyrins' absorption peaks: one at 420 nm and one in the near-infrared window at 674 nm, while one Dox absorption peak at 494 nm was excepted. The maximum excitation (Ex) and emission (Em) wavelengths of porphyrin liposomes were at ~420 nm and 680 nm, respectively.

After LIFU irradiation, pp-lipo exhibited US-triggered disruption. The sonication process facilitated progressive destruction of Dox-pp-lipo with increasing intensity (Fig. 2B) and exposure time (Fig. 2C). Dox-pp-lipo showed enhanced release where approximately 38% and 76% Dox were released after 0.2 W/cm^2 and 0.3 W/cm^2 US exposure for 60 s, respectively. Reference liposomes without Pyro-lipid did not show obvious drug release when the acoustic intensity was below 0.2 W/cm^2 and displayed some extent of drug release under 0.3 W/cm^2 stimulus, which is lower than the cargo release ratio in Dox-pp-lipo. TEM observation further indicated the disturbance of porphyrin liposomes upon LIFU trigger, showing accelerated morphological changes with increased intensity and duration time (Supporting Fig.2).

We next investigated the possible mechanisms involved in drug-release from pp-lipo under our experimental conditions (1.0 MHz, duty cycle = 5%, PRF = 1 Hz). Although the mechanism of US-mediated drug release is not well understood to date, it has been suggested to be related to either thermal or nonthermal effects. US exposure induced only a small increase in the temperature of liposome solution, excluding the thermal-effect in our treatment system. To investigate the sonosensitivity of pp-lipo, both size and distribution were investigated before and after US exposure. **Supporting Table 1** summarizes the US treated pp-lipo with a slight change towards a larger mean size, less uniformity and a broader distribution as evidenced by DLS measurement with increasing PDI. Although previous studies indicated that a sufficient mechanical index is needed to initiate drug release by using non-focused low frequency US [22–24], clinical application requires a high frequency US transducer to focus the required energy for precise therapy. Thus, this study focused on a therapeutic frequency of 1.0 MHz to initiate drug release from pp-lipo and it is expected that less acoustic energy is required to promote drug release compared to conventional liposomes. This is of great clinical importance because damage to surrounding healthy tissues and cells can thus be minimized during treatment. To verify whether US cavitational events actually took place at the utilized intensities, the presence of ·OH was detected by measuring the fluorescence intensity of an US-exposed TA solution [32]. An increase of fluorescent HTA intensity was observed with increasing exposure intensities (Supporting Fig. 3). Minimal fluorescence was detected in samples exposed to 0.15 W/cm^2, which may be below the threshold for drug release. Above this threshold, HTA fluorescence increased with increasing intensity, which indirectly suggested that cavitation was, at least partially, responsible for US triggered drug release in the designed system. To further evaluate the presence of free radicals for disrupting pp-lipo, we conducted acoustic intensity-dependent drug release experiments with or without the free radical scavenger NaN_3. The result is shown in Fig. 2D and demonstrates that addition of NaN_3 alleviated Dox release from pp-lipo to a great extent, suggesting oxidative stress to be involved in US-triggered pp-lipo disruption. Exposure to US also modified the chemical properties of exposed lipids, as demonstrated by FT-IR and MS spectra. Between 1500 and 1600 cm^{-1} in FT-IR (Fig. 3A), two weak peaks were found (see the blue dashed rectangle) in the US treatment group. However, the signal was a little low and consequently was not entirely clear whether any reaction occurred. Therefore, we next applied mass spectrum analysis to confirm this. Fig. 3B shows data supporting that oxidization kinetics under US and (*m/z* 832) may be the DOPC-oxidized species upon US exposure.

This study successfully developed pp-lipo sensitive to US exposure

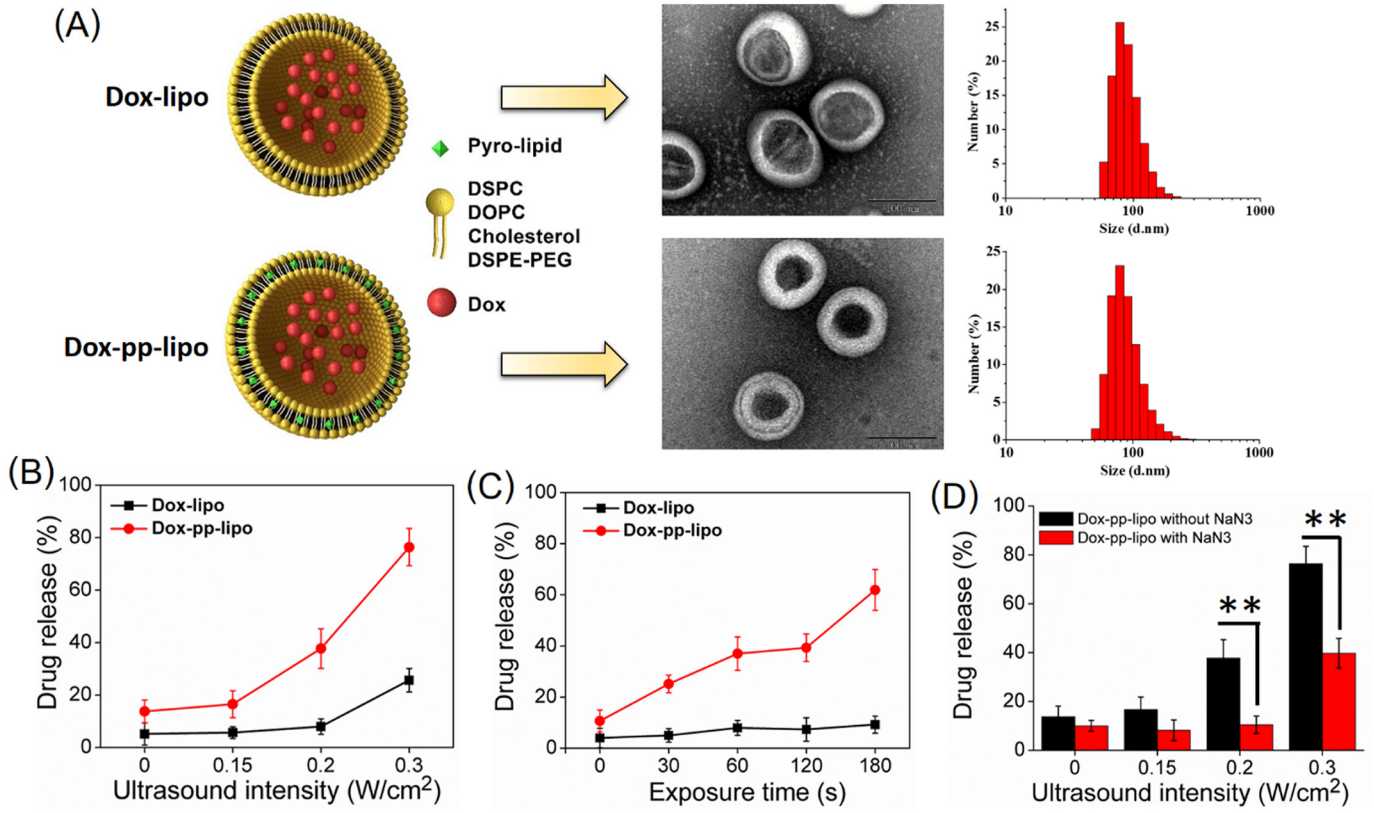

Fig. 2. Characteristics of pp-lipo and its release behavior upon ultrasound exposure. (A) Comparison of liposomes with or without 2 M% Pyro-lipid in schematic (left), TEM (middle, Bar = 100 nm) and dynamic light scattering analysis (right). (B) Dox release from pp-lipo (Dox-pp-lipo) and conventional liposome (Dox-lipo) after exposure to different acoustic intensities (0, 0.15, 0.2 and 0.3 W/cm^2) for 60 s. (C) Dox release from pp-lipo and conventional liposome after exposure to 0.2 W/cm^2 US for different durations (0, 30, 60, 120, and 180 s). (D) US triggered drug release from pp-lipo with or without the free radical scavenger NaN_3. Values are presented as mean ± SD, $n = 3$. $^{**}p < .01$ between groups.

and porphyrin presented a central role to concurrently provide ROS for liposome disruption, which may involve a sonodynamic process. The proposed cavitation upon US trigger would either lead to a sonoluminescence or other process resulting in ROS generation from the sensitizer [33, 34]. The well-aligned porphyrin-phospholipid in the lipid bilayer enabled efficient sonodynamic damage and fast drug delivery *in situ*.

3.2. Subcellular uptake, distribution, and cell toxicity under US exposure

Intracellular delivery and cell viability were assessed to confirm the chemotherapeutic effect and toxicity of pp-lipo on U87 cells, depending on the US exposure. Fig. 4 shows the intracellular distribution of Dox after 2 h of incubation with free Dox or Dox-lipo or Dox-pp-lipo. Free Dox emitted bright red fluorescence and mainly accumulated in the nuclear sites of U87 cells after 2 h of incubation. Dox-lipo and Dox-pp-lipo showed cytoplasmic distribution with weak Dox fluorescence within living cells. Dox-lipo with US exposure were more efficiently taken up by U87 cells compared to those without US exposure. However, there was no obvious differences were found in subcellular location in Dox-lipo with or without US exposure, where Dox was predominantly localized in the cytoplasm with few inside cell nuclei. While, US exposure not only enhanced the cellular uptake efficiency of Dox-pp-lipo, but also promoted the nuclear translocation of Dox, exhibiting increased Dox fluorescence in nuclear sites as well as in the cytosol. US has been suggested as a viable therapeutic strategy because

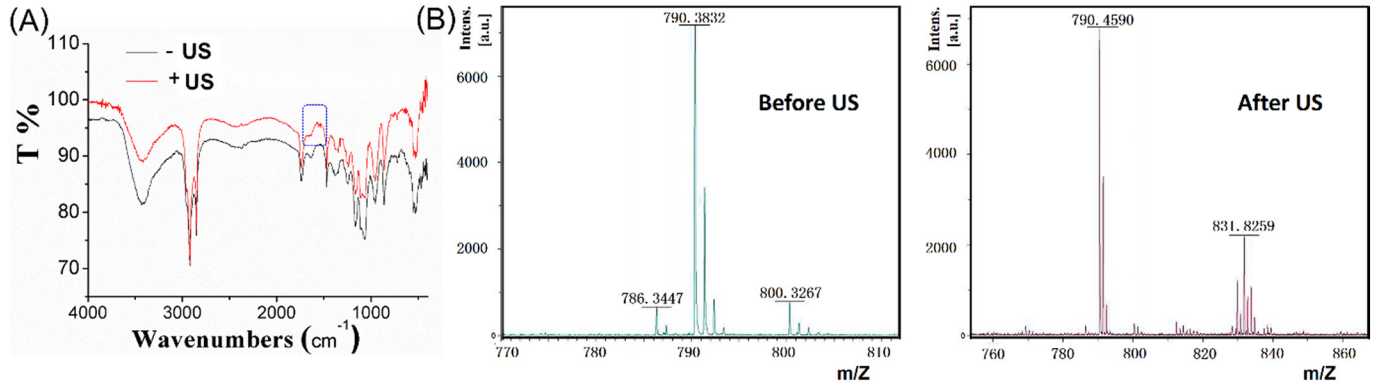

Fig. 3. Spectral changes of pp-lipo upon US treatment. (A) Infrared spectra of pp-lipo before and after US treatment (0.3 W/cm^2, 60 s duration). (B) Mass spectra of pp-lipo before and after US treatment (0.3 W/cm^2, 60 s duration).

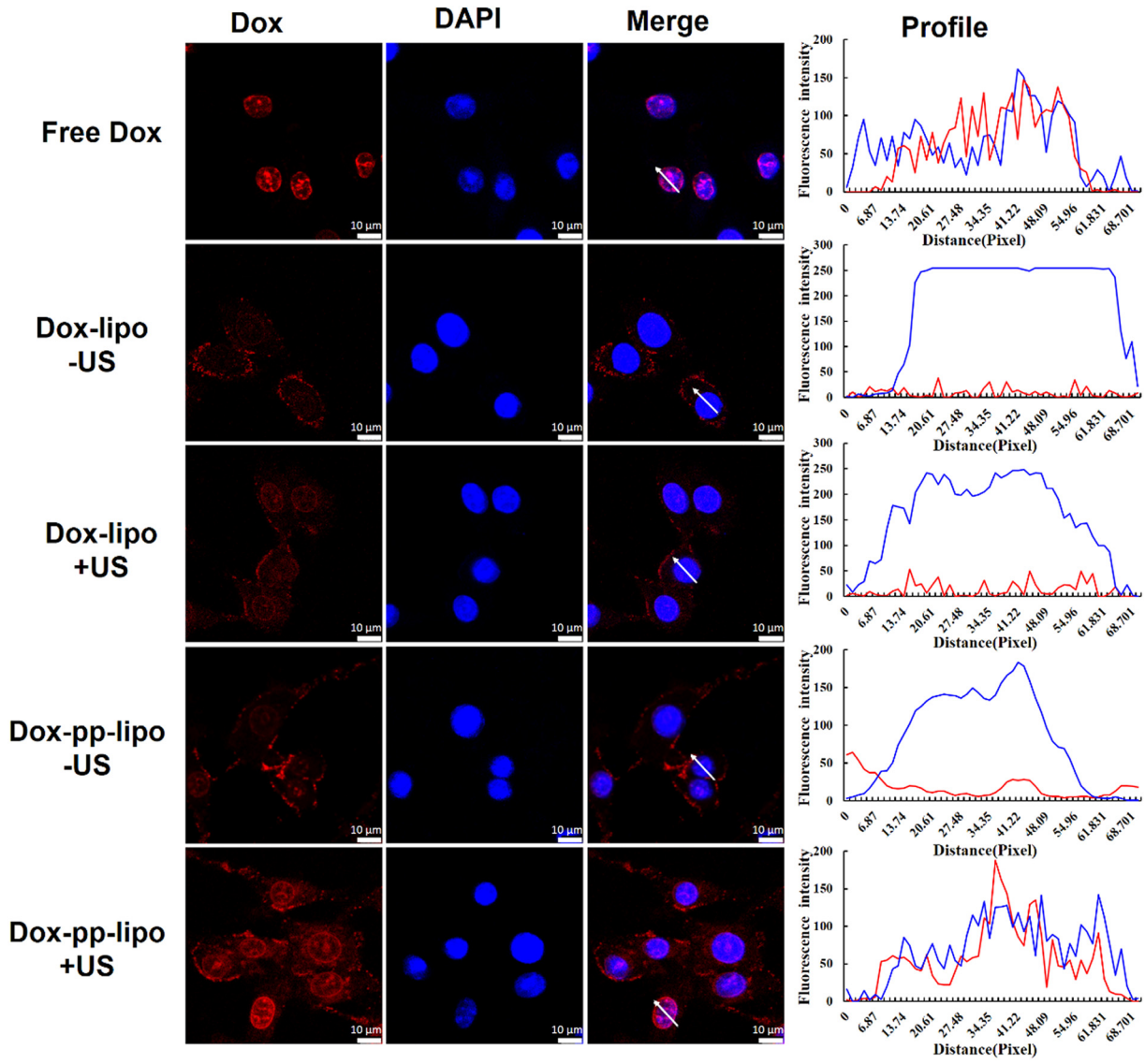

Fig. 4. Subcellular uptake of Dox upon US treatment. U87 cells were seeded in chamber slides and incubated for 2 h in Opti-MEM (Gibco) with 10 μg/ml Dox in either free or Dox-lipo or Dox-pp-lipo form, then exposed to US (0.2 W/cm^2, 60 s) prior to confocal imaging. Dox fluorescence (red) and nuclear DAPI fluorescence (blue) were captured *via* confocal microscopy. The profile on the right channel represents the fluorescence distribution as indicated sections (white arrow) in the merged channel, which shows the degree of colocalization between Dox and the nucleus. Bar = 10 μm. (For interpretation of the references to colour in this figure legend, the reader is referred to the web version of this article.)

the transient sonoporation increased the permeability of cell membranes [35, 36]. Recently, sonoporation has been investigated for its effect of enhancing intracellular drug or gene delivery [37, 38]. The increase of subcellular interactions between drugs and targeting sites benefits an improvement of the therapeutic index. Correspondingly, the present designed sono-sensitive porphyrin in the liposomes enables US to collapse liposomes, thus facilitating Dox nuclear translocation and exerting DNA damage.

To determine the US-responsive pp-lipo' biological effects in cells, we exposed U87 cells to different intensities. Fig. 5A shows that the cell viability of either group treated with free Dox, Dox-lipo or Dox-pp-lipo decreased with increasing Dox concentrations. Free Dox shows more cytotoxicity than Dox in liposomes ($p < .05$) without US treatment, and there was no statistical difference in cell viability of Dox-lipo and Dox-pp-lipo ($p > .05$). This may be related to their distinct subcellular distribution patterns as shown in Fig. 4. We then investigated the dependency of pp-lipo bioactivity on the US intensity. Treatments with 0.2 W/cm^2 and 0.3 W/cm^2 induced cytotoxicity significantly, whereas 0.15 W/cm^2 treatment did not induce cytotoxicity compared with non-US treatment group (Fig. 5B). Cell viability inhibition of pp-lipo (1 μg/ml Dox) was greatly enhanced upon US exposure, representing up to four-fold increased potencies under 0.3 W/cm^2 trigger than without US trigger. In comparison, the intensity-dependency of Dox-lipo was not significantly responsive (Fig. 5C). Furthermore, the toxicity of Dox-pp-lipo depending on US intensity was demonstrated *via* calcein AM/PI staining (Fig. 5D). Here, the increased intracellular ROS level was quantitatively determined using flow cytometry (Fig. 5E). US alone did not show much toxicity without the presence of Dox-pp-lipo (Supporting Figs. 4 and 5). These findings indicate that the pp-lipo biological effects could not only be controlled (whether exposed to US or not), but also tuned by varying the US intensity.

3.3. DNA damage in vitro in an intensity-dependent manner

We investigated the US-dependency of pp-lipo induced cytotoxicity focusing on DNA damage *in vitro*. Comet assay based on smaller DNA fragments migrate faster in an electric field and the pattern of migration produces a profile resembling the shape of a comet. Fig. 6 shows that

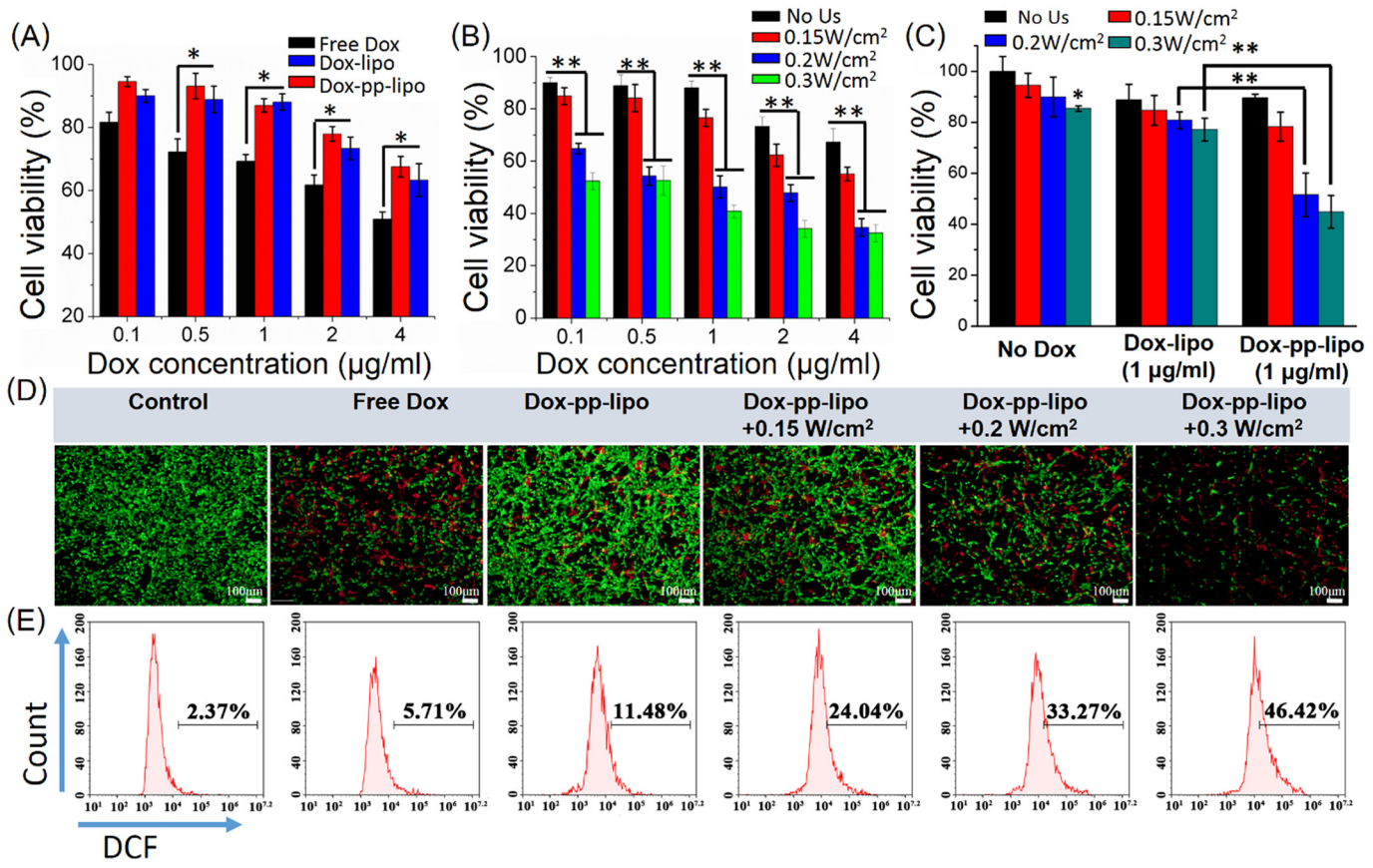

Fig. 5. Cell toxicity of Dox in distinct forms upon US treatment. (A) Cell viability of U87 cells after incubation with Dox in either free or Dox-lipo or pp-lipo, assessed 24 h after exposure using the CCK-8 assay. Values are given as mean ± S.D., $n = 4$. $^{*}p < .05$, between groups. (B) Dox-pp-lipo induced cell viability loss with or without US exposure. $^{**}p < .01$ between groups. (C) Comparison of cell viability of U87 cells by Dox-lipo and Dox-pp-lipo after different US treatments. $^{**}p < .01$ between groups. (D) Cytotoxicity of pp-lipo can be turned by choosing the intensity of the applied US, as measured by Calcein AM/PI double staining. Viable cells were stained green with calcein-AM, and damaged cells were stained red with PI. (Bar = 100 μm) (E) Intracellular ROS generation as measured by flow cytometry. The representative figures are shown. (For interpretation of the references to colour in this figure legend, the reader is referred to the web version of this article.)

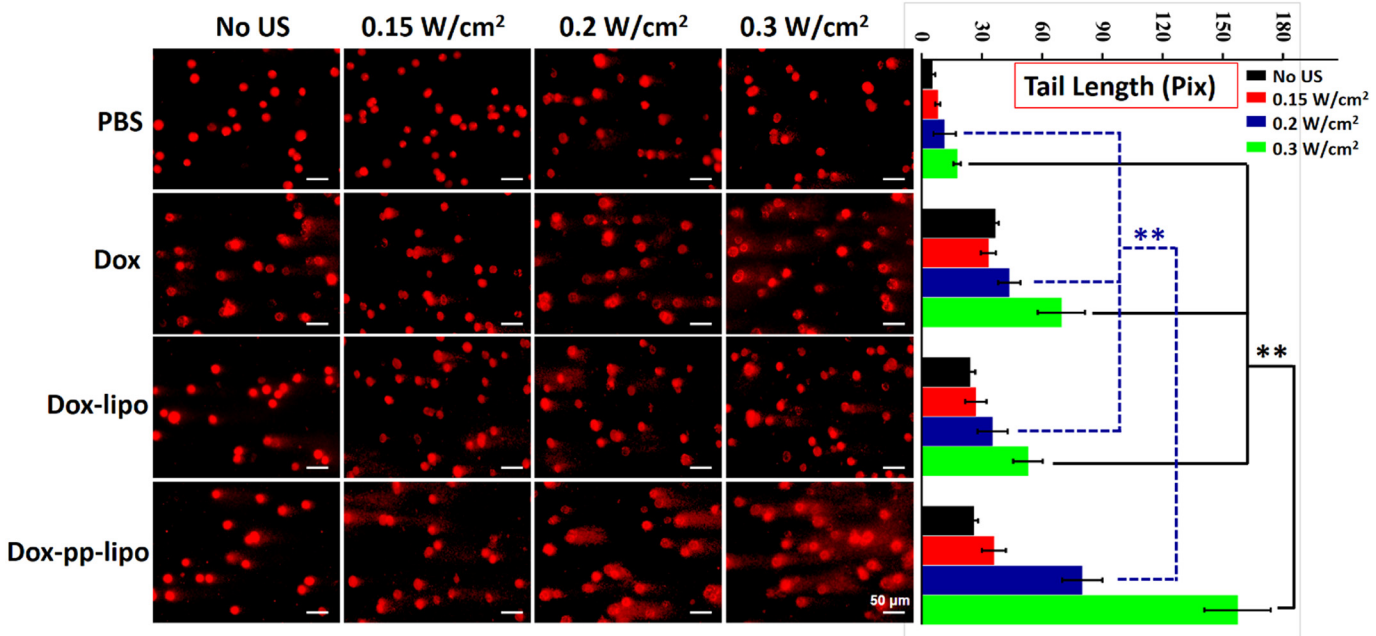

Fig. 6. pp-lipo induced DNA damage *in vitro* upon US exposure. The US-dependent induction of DNA damage in Dox-pp-lipo was evaluated by comet assay. Representative fluorescence images are shown in the left and the tail length was calculated by CASP software (right). $^{**}p < .01$, between groups.

the untreated cells of control retained their normal nucleus morphology with very short tail length. Gradually longer comet tails were captured after either free Dox or liposomal Dox treatment, where the former was more obvious than the latter. US alone produced little DNA damage, while slightly increasing Dox and Dox-lipo caused DNA damage. However, DNA fragmentation was particularly pronounced in the Dox-pp-lipo plus US regime, which showed a US intensity dependent manner, matching the cell viability values obtained in cytotoxicity assays. These results support the interpretation that Dox-pp-lipo potently induce DNA damage *in situ* upon US exposure, which is presumably linked to the activation of sonosensitization induced oxidation and the effective disruption of liposomes, facilitating Dox trafficking into the cell nuclei. This experiment also suggests that pp-lipo can be used as an US-responsive platform to precisely regulate DNA damage *in situ*.

3.4. LIFU triggered drug release in vivo

Due to the EPR effect, most nanoparticles with diameters of approximately 100 nm are typically able to cross the capillary wall and accumulate in the tumor interstitium [39]. However, this does not enable uniform delivery of nanoparticles to all parts of tumors at sufficient quantities. Large areas of the tumor are typically not reached since the tumor vessels are highly heterogeneous in their spatial distribution and the interstitial matrix is abnormal with hypertension in some places but not in others [40]. This is highly challenging for the control of localized drug-release and the deep and uniform penetration of intravenously administrated nanoparticles, which are required to obtain a sufficient drug concentration at the target site. US is of particular interest because it is noninvasive, can be controlled both spatially and temporally, and can penetrate deeply into the body. It has been indicated that US increases the permeability of blood-tissue barriers and cell membranes, thus improving both the release and the distribution of drugs [41, 42]. Animal studies using US and liposomal drugs also demonstrated a reduced tumor growth rate compared to the administration of liposomal drugs alone [43]. We next explored the feasibility of targeted delivery *in vivo* with pp-lipo in response to a LIFU trigger.

Porphyrin-loaded liposomes have been described for various biological applications and the fluorescence imaging of porphyrin could serve as a sensitive tool to track drug delivery. The *in vitro* studies described above have demonstrated the pyro-lipid facilitated drug release from pp-lipo in response to US treatment. We assessed whether US exposure could also trigger drug release *in situ*. BALB/c nude mice xenografted with bilateral U87 tumors were used in this *in vivo* study. Fig. 7A shows that no significant fluorescence signal was obtained in tumors during the first few hours following intravenous injection, after 12–24 h injection, tumors exhibited porphyrin fluorescence enabling clear delineation from normal tissues. This suggests that pp-lipo potentially accumulated in the tumor through enhanced permeability and retention. US enhanced the porphyrin fluorescence signal 12 h after intravenous injection of pp-lipo, which was monitored as a function of intensity. Increased porphyrin fluorescence in the left tumor highlights the region that was enhanced by US exposure compared to their auto-right control without US treatment (Fig. 7B). This result implies that *in situ* regulation of pp-lipo could be influenced by US exposure. Furthermore, tumors were dissected and subjected to *ex vivo* Dox-fluorescence imaging. Dox is a popular agent for the exploration of drug-release patterns due to its inherent fluorescence allowing visualization of drug distribution in various tissues or cells. Moreover, Dox fluorescence is self-quenched at high concentrations of its molecular dissolved form. In contrast, Dox fluorescence is increased after binding the histones, DNA, and phospholipids [44]. Stereo fluorescence microscopic observation (Supporting Fig. 6) shows that US-treated tumors displayed a far more intense and diffuse Dox-fluorescence compared to untreated specimens, suggesting that not only effective disruption of pp-lipo and triggering release of cargos, but also deep diffusion of chemotherapeutic agents in the tumor. However, reaching the target site is not a guarantee that the transported drug will be effective, as most chemotherapeutic drug need to enter specific cellular sites, *e.g.*, alkylating agents need to be transported into nuclei to act on DNA molecules. Consequently, fluorescence tumors were subjected to histologic section analysis (Fig. 7C), which showed an increased and diffused pattern of Dox-fluorescence after US exposure, and the Dox fluorescence penetrated into cell nuclei. This phenomenon was predominant for a US intensity above 0.2 W/cm^2. In contrast, sections of tumors not exposed to US displayed far lower fluorescent signals, which were rarely detected in nuclei sites of tumor cells. These results suggest that pp-lipo plays an active role in allowing the intracellular diffusion of drug release to perform DNA damage *in situ*. Furthermore, semi-quantitative biodistribution analysis of each excised organ was performed by using region-of-interest analysis at 12 h after liposome administration, followed by different US treatments. US exposure increased Dox fluorescent imaging in tumor tissues (Fig. 7D, E) while causing no visible effect on the liver, in which liposomal delivery greatly decreased possible hepatotoxcity induced by free Dox. Therefore, the local delivery of pp-lipo based on US cavitation and sonochemical effects might enhance tumor vascular permeability and thus enrich sufficient amounts of therapeutics, while producing little adverse effects on normal tissues.

3.5. Anti-tumor efficacy

To evaluate the anti-tumor efficacy *in vivo*, U87 cells were inoculated into the thigh of nude mice. The tumor-bearing mice were exposed to US for 3 min 12 h after i.v. injection with either liposomal or Free Dox. The presence of porphyrin-phospholipid also exhibited an important role in inhibiting tumor growth *in vivo* (Supporting Fig. 7), in which US significantly enhanced Dox-pp-lipo induced tumor volume inhibition; however, it did not work well for both free Dox and Dox-lipo injection (Dox, 5 mg/kg; Us, 0.2 W/cm^2). This was consistent with a previous report that indicated that porphyrin-based nanoparticles with Dox encapsulation did not show significant effect compared to equivalent free Dox, whereas porphyrin-based nanoparticles were greatly activated by the specific stimulus and induced significant cytotoxicity [45]. Next, we used different Dox doses (2.5 and 5 mg/kg) and US intensities (0.2 and 0.3 W/cm^2) to explore drug delivery potency of pp-lipo and the synergistic sonochemotherapeutics. In summary, the groups under Dox-pp-lipo plus US treatment exhibited statistically significant antitumor efficacy. The induced tumor growth inhibition increased with increasing Dox amount and US intensity (Fig. 8A). Dox alone (5 mg/kg) did not show any tumor inhibition compared to saline control. When empty-pp-lipo was applied with US irradiation, tumor growth was inhibited to some extent, but growth was sustained as days progressed. The partial suppression was likely induced by the sonodynamic reaction by US activation of porphyrin in the liposomes [46]. Both US triggering sonochemical and chemotherapeutic effects concurrently contributed to the effective antitumor efficacy observed in the Dox-pp-lipo plus US group [47]. The *in vivo* inhibition also suggests the suitability of pp-lipo for acoustically defined drug release *in situ*. Kaplan-Meier survival curves (Fig. 8B) demonstrate a prolonged survival time of Dox-pp-lipo (5 mg/kg) in treatment with 0.2 W/cm^2 and 0.3 W/cm^2. The medium survival time of U87 bearing mice that were treated with Dox-pp-lipo (5 mg/kg) plus 0.2 W/cm^2 was prolonged by 26 days and 23 days compared to saline and free Dox groups, respectively.

Therapeutic efficacy was further evaluated *via* staining of tumor sections. The HE staining shown in Fig. 8C exhibited high cell-density of tumor tissue in the saline-treated group as well as the lack of variations in free Dox or 0.3 W/cm^2 US treated groups; however, HE staining in the empty-pp-lipo plus 0.3 W/cm^2 group was relatively sparse. The highest decrease of tumor area was observed in the combined Dox-pp-lipo and US treatment group with obvious vacant sections and condensed nuclear staining, indicating increased therapeutic outcome *in vivo* as a result of increased Dox dose and US intensity. PCNA positive

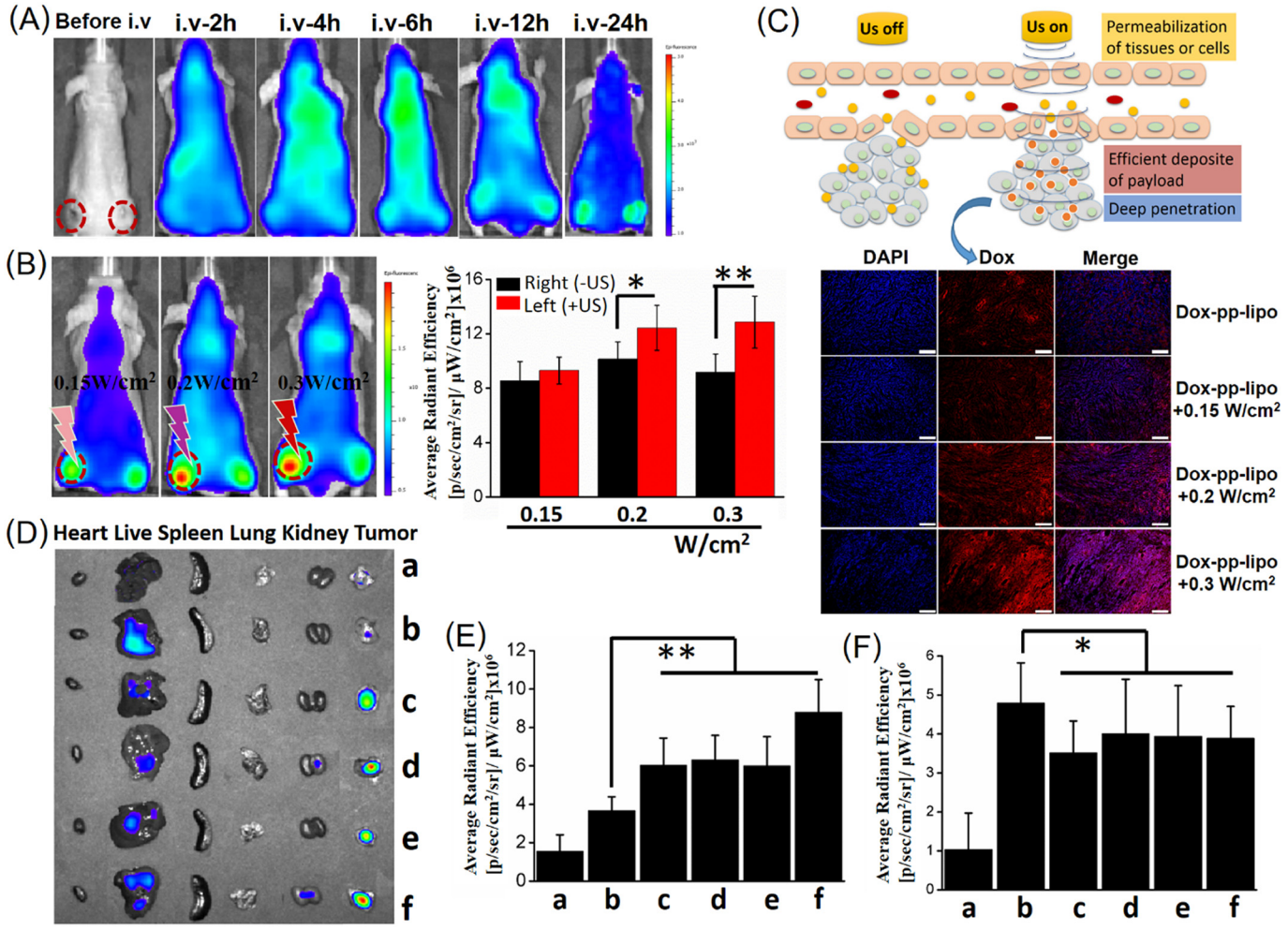

Fig. 7. LIFU triggered drug delivery *in vivo*. (A) *In vivo* fluorescence imaging of pp-lipo in nude mice-bearing U87 tumors after i.v injection. Red circles indicate bilateral tumors. (B) Porphyrin fluorescent signals with or without US exposure at 12 h post i.v injection of pp-lipo. Left side tumors were exposed to US, while right side tumors without US exposure were used for comparison. The column graph in the right panel indicates average fluorescence intensity changes. $*p < .05$, $**p < .01$, between groups. (C) US-assisted intratumoral drug delivery and penetration after i.v. injection with Dox-pp-lipo. Dox fluorescence images of tumor sections of mice injected with Dox-pp-lipo and exposure to a specific US intensity 12 h later. Bar = 100 μm. (D) *Ex vivo* images of Dox content in tumors and major organs after different treatments. (E) and (F) indicate the calculated average fluorescence intensity in the tumor (E) and liver (F), respectively. $*p < .05$, $**p < .01$, between groups. a, PBS; b, free Dox (5 mg/kg); c, Dox-pp-lipo (2.5 mg/kg) + 0.2 W/cm^2; d, Dox-pp-lipo (2.5 mg/kg) + 0.3 W/cm^2; e, Dox-pp-lipo (5 mg/kg) + 0.2 W/cm^2; f, Dox-pp-lipo (5 mg/kg) + 0.3 W/cm^2. (For interpretation of the references to colour in this figure legend, the reader is referred to the web version of this article.)

staining also showed similar reduction tendency (Fig. 8D). The acoustically controlled pp-lipo DNA damage *in vivo* was demonstrated using TUNEL assay (Fig. 8E). The most severe DNA damage was found in Dox-pp-lipo (5 mg/kg Dox) and 0.3 W/cm^2 combined group, in which US treatment assisted liposomes in releasing the loaded drug. This favored broad drug diffusion in the tumor, thus improving DNA damage *in situ* and optimizing benefits in therapeutic efficiency. Such sono-regulatable local release benefits from one point that sonodynamic oxidization disrupts liposome membrane, and for another, the mechanical energy of US improves nanomedicine penetration into deep tumor region [48, 49]. For the toxic evaluation, tumor-bearing mice still gained weight after different treatments, and no histological damage was observed in several major organs (Supporting Fig. 8).

4. Conclusions

With the use of pp-lipo, effective and on-demand drug delivery has been demonstrated in a sonodynamic-dependent manner both *in vitro* and *in vivo*. This drug release *via* pp-lipo shows good potential for US triggered controlling liposomal drug release and provides a promising platform for the delivery of therapeutics to tumors. Further optimization of US exposure parameters is required to facilitate future applications.

Acknowledgements

The research received support from the National Natural Science Foundation of China (81472846, 81571834, 11534013, 81527901), the Major State Basic Research Development Program of China (973 Program) (2015CB755500), Key Laboratory for Magnetic Resonance and Multimodality Imaging of Guangdong Province (2014B030301013), National Institutes of Health (R01EB017270, DP5OD017898), Shenzhen Science and Technology Innovation Committee (JCYJ20170307165254568), the Innovative Talents Promotion Plan in Shaanxi Province (2017KJXX-78), and the Academic Leaders and Academic Backbones, Shaanxi Normal University (16QNGG012).

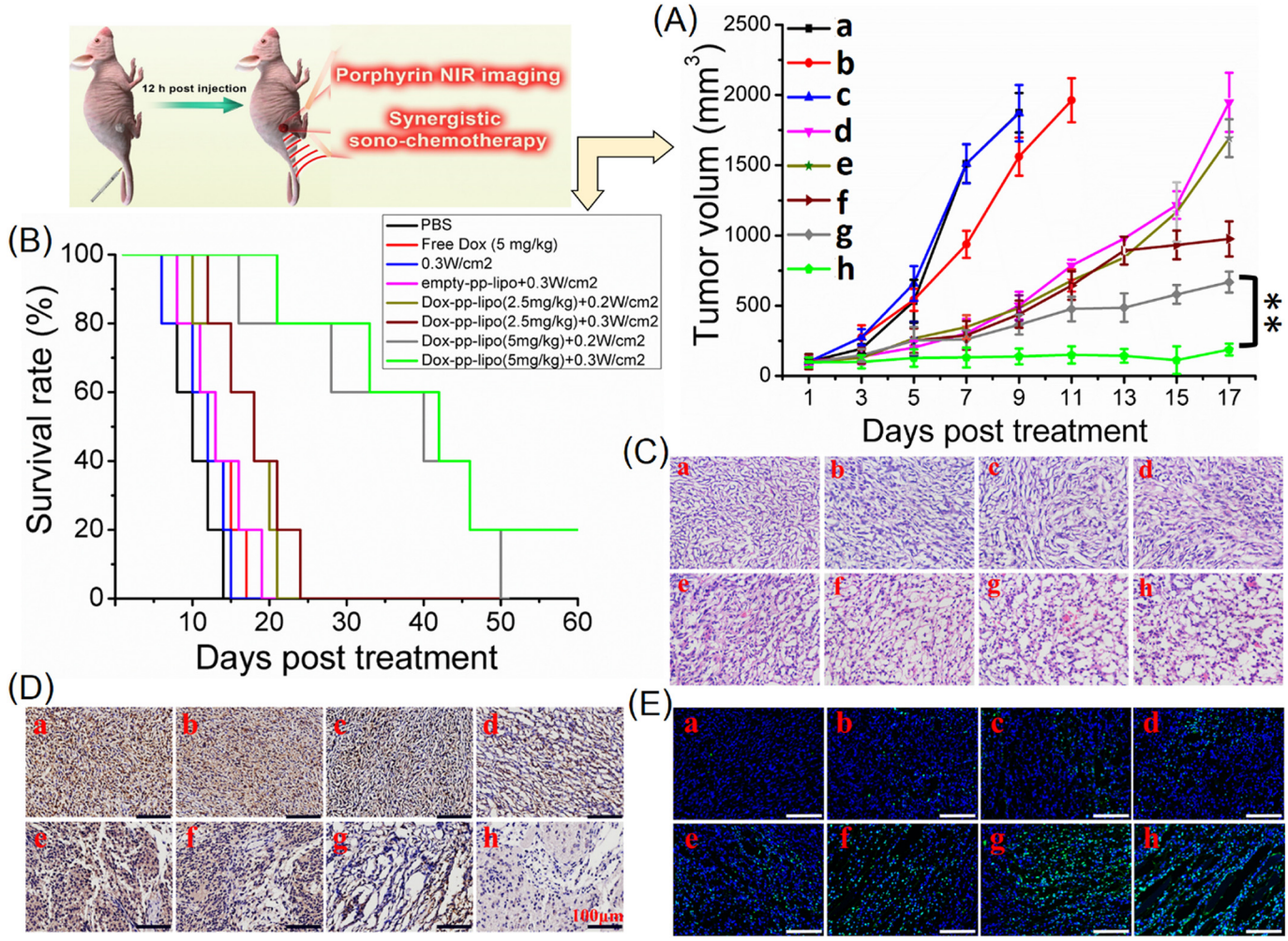

Fig. 8. ***In vivo*** **cancer sonochemotherapy in xenograft mice model with U87 cells**. (A) Tumor growth curves of different groups of U87 tumor-bearing mice ($n = 7$). $^{**}p < .01$. (B) Survival rates of mice bearing U87 tumors after different treatments. (C) HE staining images of tumor sections collected from different treated groups of mice 24 h post treatment (400×). (D) PCNA staining of tumor tissues. The nuclei were stained with DAPI (blue). Bar = 100 μm. (E) US-improved DNA damage *in situ* by TUNEL assay at 24 h post treatment. The cell nuclei were counterstained with DAPI (blue). Bar = 100 μm. a, PBS; b, free Dox (5 mg/kg); c, 0.3 W/cm^2; d, empty-pp-lipo + 0.3 W/cm^2; e, Dox-pp-lipo (2.5 mg/kg) + 0.2 W/cm^2; f, Dox-pp-lipo (2.5 mg/kg) + 0.3 W/cm^2; g, Dox-pp-lipo (5 mg/kg) + 0.2 W/cm^2; h, Dox-pp-lipo (5 mg/kg) + 0.3 W/cm^2. (For interpretation of the references to colour in this figure legend, the reader is referred to the web version of this article.)

Appendix A. Supplementary data

Supplementary data to this article can be found online at https://doi.org/10.1016/j.jconrel.2018.07.048.

References

[1] R.A. El-Awady, M.H. Semreen, M.M. Saber-Ayad, F. Cyprian, V. Menon, T.H. Al-Tel, Modulation of DNA damage response and induction of apoptosis mediates synergism between doxorubicin and a new imidazopyridine derivative in breast and lung cancer cells, DNA Repair 37 (2016) 1–11.

[2] J.V. McGowan, R. Chung, A. Maulik, I. Piotrowska, J.M. Walker, D.M. Yellon, Anthracycline chemotherapy and cardiotoxicity, Cardiovasc. Drugs Ther. 31 (2017) 63–75.

[3] M. Cagel, E. Grotz, E. Bernabeu, M.A. Moretton, D.A. Chiappetta, Doxorubicin: Nanotechnological overviews from bench to bedside, Drug Discov. Today 22 (2017) 270–281.

[4] T.M. Allen, P.R. Cullis, Liposomal drug delivery systems: from concept to clinical applications, Adv. Drug Deliv. Rev. 65 (2013) 36–48.

[5] Y. Barenholz, Doxil®-the first FDA-approved nano-drug: lessons learned, J. Control. Release 160 (2012) 117–134.

[6] Q. Chen, H. Ke, Z. Dai, Z. Liu, Nanoscale theranostics for physical stimulus-responsive cancer therapies, Biomaterials 73 (2015) 214–230.

[7] Y. Wang, M.S. Shim, N.S. Levinson, H.W. Sung, Y. Xia, Stimuli-responsive materials for controlled release of theranostic agents, Adv. Funct. Mater. 24 (2014) 4206–4220.

[8] F. Li, J. Lu, X. Kong, T. Hyeon, D. Ling, Dynamic nanoparticle assemblies for biomedical applications, Adv. Mater. 29 (2017) 1605897.

[9] N. Zhao, B. Wu, X. Hu, D. Xing, NIR-triggered high-efficient photodynamic and chemo-cascade therapy using caspase-3 responsive functionalized upconversion nanoparticles, Biomaterials 141 (2017) 40–49.

[10] A. Bansal, Y. Zhang, Photocontrolled nanoparticle delivery systems for biomedical applications, Acc. Chem. Res. 47 (2014) 3052–3060.

[11] R.J. Paproski, A. Forbrich, E. Huynh, J. Chen, J.D. Lewis, G. Zheng, R.J. Zemp, Porphyrin nanodroplets: sub-micrometer ultrasound and photoacoustic contrast imaging agents, Small 12 (2016) 371–380.

[12] Y. Zhou, X. Liang, Z. Dai, Porphyrin-loaded nanoparticles for cancer theranostics, Nanoscale 8 (2016) 12394–12405.

[13] J.F. Lovell, C.S. Jin, E. Huynh, H. Jin, C. Kim, J.L. Rubinstein, W.C. Chan, W. Cao, L.V. Wang, G. Zheng, Porphysome nanovesicles generated by porphyrin bilayers for use as multimodal biophotonic contrast agents, Nat. Mater. 10 (2011) 324–332.

[14] K.A. Carter, S. Shao, M.I. Hoopes, D. Luo, B. Ahsan, V.M. Grigoryants, W. Song, H. Huang, G. Zhang, R.K. Pandey, J. Geng, B.A. Pfeifer, C.P. Scholes, J. Ortega, M. Karttunen, J.F. Lovell, Porphyrin-phospholipid liposomes permeabilized by near-infrared light, Nat. Commun. 5 (2014) 3546.

[15] M.S. Valic, G. Zheng, Rethinking translational nanomedicine: insights from the 'bottom-up' design of the porphysome for guiding the clinical development of imageable nanomaterials, Curr. Opin. Chem. Biol. 33 (2016) 126–134.

[16] D. Luo, N. Li, K.A. Carter, C. Lin, J. Geng, S. Shao, W.C. Huang, Y. Qin, G.E. Atilla-Gokcumen, J.F. Lovell, Rapid light-triggered drug release in liposomes containing small amounts of unsaturated and porphyrin-phospholipids, Small 12 (2016) 3039–3047.

[17] D. Luo, K.A. Carter, A. Razi, J. Geng, S. Shao, D. Giraldo, U. Sunar, J. Ortega, J.F. Lovell, Doxorubicin encapsulated in stealth liposomes conferred with light-triggered drug release, Biomaterials 75 (2016) 193–202.

[18] X. Ai, J. Mu, B. Xing, Recent advances of light-mediated theranostics, Theranostics 6

(2016) 2439–2457.
[19] M. Postema, O.H. Gilja, Ultrasound-directed drug delivery, Curr. Pharm. Biotechnol. 8 (2007) 355–361.
[20] E.S. Ebbini, G. ter Haar, Ultrasound-guided therapeutic focused ultrasound: current status and future directions, Int. J. Hyperth. 31 (2015) 77–89.
[21] S.R. Sirsi, M.A. Borden, State-of-the-art materials for ultrasound-triggered drug delivery, Adv. Drug Deliv. Rev. 72 (2014) 3–14.
[22] G.A. Husseini, M.A. Diaz De La Rosa, E.S. Richardson, D.A. Christensen, W.G. Pitt, The role of cavitation in acoustically activated drug delivery, J. Control. Release 107 (2005) 253–261.
[23] A. Schroeder, Y. Avnir, S. Weisman, Y. Najajreh, A. Gabizon, Y. Talmon, J. Kost, Y. Barenholz, Controlling liposomal drug release with low frequency ultrasound: mechanism and feasibility, Langmuir 23 (2007) 4019–4025.
[24] S.E. Ahmed, A.M. Martins, G.A. Husseini, The use of ultrasound to release chemotherapeutic drugs from micelles and liposomes, J. Drug Target. 23 (2015) 16–42.
[25] T.J. Evjen, E.A. Nilssen, S. Rögnvaldsson, M. Brandl, S.L. Fossheim, Distearoylphosphatidylethanolamine-based liposomes for ultrasound-mediated drug delivery, Eur. J. Pharm. Biopharm. 75 (2010) 327–333.
[26] P. Huang, X. Qian, Y. Chen, L. Yu, H. Lin, L. Wang, Y. Zhu, J. Shi, Metalloporphyrin-encapsulated biodegradable nanosystems for highly efficient magnetic resonance imaging-guided sonodynamic cancer therapy, J. Am. Chem. Soc. 139 (2017) 1275–1284.
[27] X. Qian, Y. Zheng, Y. Chen, Micro/nanoparticle-augmented sonodynamic therapy (SDT): breaking the depth shallow of photoactivation, Adv. Mater. 28 (2016) 8097–8129.
[28] G. Haran, R. Cohen, L.K. Bar, Y. Barenholz, Transmembrane ammonium sulfate gradients in liposomes produce efficient and stableentrapment of amphipathic weak bases, Biochim. Biophys. Acta 2 (1993) 201–215.
[29] V. Garaj-Vrhovac, N. Kopjar, The alkaline comet assay as biomarker in assessment of DNA damage in medical personnel occupationally exposed to ionizing radiation, Mutagenesis 18 (2003) 265–271.
[30] X. Wang, J. Hu, P. Wang, S. Zhang, Y. Liu, W. Xiong, Q. Liu, Analysis of the in vivo and in vitro effects of photodynamic therapy on breast cancer by using a sensitizer, sinoporphyrin sodium, Theranostics 5 (2015) 772–786.
[31] T.J. Mason, Therapeutic ultrasound an overview, Ultrason. Sonochem. 18 (2011) 847–852.
[32] L. Somaglino, G. Bouchoux, J.L. Mestas, C. Lafon, Validation of an acoustic cavitation dose with hydroxyl radical production generated by inertial cavitation in pulsed mode: application to in vitro drug release from liposomes, Ultrason. Sonochem. 18 (2011) 577–588.
[33] X. Wang, Y. Jia, P. Wang, Q. Liu, H. Zheng, Current status and future perspectives of sonodynamic therapy in glioma treatment, Ultrason. Sonochem. 37 (2017) 592–599.
[34] E. Huynh, B.Y. Leung, B.L. Helfield, M. Shakiba, J.A. Gandier, C.S. Jin, E.R. Master, B.C. Wilson, D.E. Goertz, G. Zheng, In situ conversion of porphyrin microbubbles to nanoparticles for multimodality imaging, Nat. Nanotechnol. 10 (2015) 325–332.
[35] P. Wu, Y. Jia, F. Qu, Y. Sun, P. Wang, K. Zhang, C. Xu, Q. Liu, X. Wang, Ultrasound-responsive polymeric micelles for sonoporation-assisted site-specific therapeutic action, ACS Appl. Mater. Interfaces 9 (2017) 25706–25716.
[36] B. Helfield, X. Chen, S.C. Watkins, F.S. Villanueva, Biophysical insight into mechanisms of sonoporation, Proc. Natl. Acad. Sci. U. S. A. 113 (2016) 9983–9988.
[37] A. Delalande, S. Kotopoulis, M. Postema, P. Midoux, C. Pichon, Sonoporation: mechanistic insights and ongoing challenges for gene transfer, Gene 525 (2013) 191–199.
[38] A.Y. Rwei, J.L. Paris, B. Wang, W. Wang, C.D. Axon, M. Vallet-Regí, R. Langer, S. Daniel, D.S. Kohane, Ultrasound-triggered local anaesthesia, Nat. Biomed. Eng. 1 (2017) 644–653.
[39] A.I. Minchinton, I.F. Tannock, Drug penetration in solid tumours, Nat. Rev. Cancer 6 (2006) 583–592.
[40] R.K. Jain, T. Stylianopoulos, Delivering nanomedicine to solid tumors, Nat. Rev. Clin. Oncol. 7 (2010) 653–664.
[41] H. Moon, J. Kang, C. Sim, J. Kim, H. Lee, J.H. Chang, H. Kim, Multifunctional theranostic contrast agent for photoacoustics- and ultrasound-based tumor diagnosis and ultrasound-stimulated local tumor therapy, J. Control. Release 218 (2015) 63–71.
[42] B. Kang, M.B. Zheng, P. Song, A.P. Chen, J.W. Wei, J.J. Xu, Y. Shi, H.Y. Chen, Subcellular-scale drug transport via ultrasound-degradable mesoporous nanosilicon to bypass cancer drug resistance, Small 13 (2017) 1604228.
[43] A. Schroeder, R. Honen, K. Turjeman, A. Gabizon, J. Kost, Y. Barenholz, Ultrasound triggered release of cisplatin from liposomes in murine tumors, J. Control. Release 137 (2009) 63–68.
[44] P. Mohan, N. Rapoport, Doxorubicin as a molecular nanotheranostic agent: effect of doxorubicin encapsulation in micelles or nanoemulsions on the ultrasound-mediated intracellular delivery and nuclear trafficking, Mol. Pharm. 7 (2010) 1959–1973.
[45] H. Park, W. Park, K. Na, Doxorubicin loaded singlet-oxygen producible polymeric micelle based on chlorine e6 conjugated pluronic F127 for overcoming drug resistance in cancer, Biomaterials 35 (2014) 7963–7969.
[46] Z.J. Dai, S. Li, J. Gao, X.N. Xu, W.F. Lu, S. Lin, X.J. Wang, Sonodynamic therapy (SDT): a novel treatment of cancer based on sonosensitizer liposome as a new drug carrier, Med. Hypotheses 80 (2013) 300–302.
[47] B.H. Lammertink, C. Bos, R. Deckers, G. Storm, C.T. Moonen, J.M. Escoffre, Sonochemotherapy: from bench to bedside, Front. Pharmacol. 6 (2015) 138.
[48] F. Giuntini, F. Foglietta, A.M. Marucco, A. Troia, N.V. Dezhkunov, A. Pozzoli, G. Durando, I. Fenoglio, L. Serpe, R. Canaparo, Insight into ultrasound-mediated reactive oxygen species generation by various metal-porphyrin complexes, Free Radic. Biol. Med. 121 (2018) 190–201.
[49] H. Lee, J. Han, H. Shin, H. Han, K. Na, H. Kim, Combination of chemotherapy and photodynamic therapy for cancer treatment with sonoporation effects, J. Control. Release 283 (2018) 190–199.